

Spinon Fermi surface spin liquid in a triangular lattice antiferromagnet NaYbSe_2

Peng-Ling Dai^{#,1} Gaoning Zhang^{#,2} Yaofeng Xie,³ Chunruo Duan,³ Yonghao Gao,⁴
 Zihao Zhu,⁴ Erxi Feng,⁵ Chien-Lung Huang,³ Huibo Cao,⁵ Andrey Podlesnyak,⁵ Garrett
 E. Granroth,⁵ David Voneshen,^{6,7} Shun Wang,⁸ Guotai Tan,¹ Emilia Morosan,³ Xia
 Wang,² Lei Shu,⁴ Gang Chen,^{9,4,*} Yanfeng Guo,^{2,†} Xingye Lu,^{1,‡} and Pengcheng Dai^{3,§}

¹*Center for Advanced Quantum Studies and Department of Physics,
 Beijing Normal University, Beijing 100875, China*

²*School of Physical Science and Technology,
 ShanghaiTech University, Shanghai 201210, China*

³*Department of Physics and Astronomy, Rice University, Houston, TX 77005, USA*

⁴*State Key Laboratory of Surface Physics, Department of Physics, Fudan University, Shanghai 200433, China*

⁵*Neutron Scattering Division, Oak Ridge National Laboratory, Oak Ridge, TN 37831*

⁶*ISIS Facility, Rutherford Appleton Laboratory,
 Chilton, Didcot, Oxfordshire OX11 0QX, UK*

⁷*Department of Physics, Royal Holloway University of London, Egham, TW20 0EX, UK*

⁸*School of Physics, Huazhong University of Science and Technology, Wuhan 430074, China*

⁹*Department of Physics and HKU-UCAS Joint Institute for Theoretical and Computational Physics at Hong Kong,
 The University of Hong Kong, Hong Kong, China*

(Dated: November 19, 2021)

Triangular lattice of rare-earth ions with interacting effective spin-1/2 local moments is an ideal platform to explore the physics of quantum spin liquids (QSLs) in the presence of strong spin-orbit coupling, crystal electric fields, and geometrical frustration. The Yb delafossites, NaYbCh_2 (Ch=O, S, Se) with Yb ions forming a perfect triangular lattice, have been suggested to be candidates for QSLs. Previous thermodynamics, nuclear magnetic resonance, and muon spin rotation measurements on NaYbCh_2 have supported the suggestion of the QSL ground states. The key signature of a QSL, the spin excitation continuum, arising from the spin quantum number fractionalization, has not been observed. Here we perform both elastic and inelastic neutron scattering measurements as well as detailed thermodynamic measurements on high-quality single crystalline NaYbSe_2 samples to confirm the absence of long-range magnetic order down to 40 mK, and further reveal a clear signature of magnetic excitation continuum extending from 0.1 to 2.5 meV. By comparing the structure of our magnetic excitation spectra with the theoretical expectation from the spinon continuum, we conclude that the ground state of NaYbSe_2 is a QSL with a spinon Fermi surface.

Introduction. The quantum spin liquid (QSL) is a correlated quantum state in a solid where the spins of the unpaired electrons are highly entangled over long distances, yet they do not exhibit any long-range

magnetic order in the zero temperature limit. Originally proposed by P. W. Anderson as the ground state for a system of $S = 1/2$ spins on a two-dimensional (2D) triangular lattice that interact antiferromagnetically with their nearest neighbors [1], a QSL is a novel quantum state of matter beyond the traditional Landau's symmetry breaking paradigm [2–5], and might be relevant for our understanding of high-temperature superconductivity [6–8] and quantum computation in certain cases [9, 10]. Beyond the simple characterization of absence of a magnetic order, one key signature of the excitations in a QSL is the presence of deconfined spinons that are fractionalized quasiparticles carrying spin-1/2, observed by inelastic neutron scattering as a spin excitation continuum fundamentally different from the integer spin wave excitations in an ordered magnet [11–16].

Although spin excitation continuum has been observed in the geometrically frustrated $S = 1/2$ single crystal systems with 2D Kagomé [11], 2D triangular [12, 13], three-dimensional (3D) distorted Kagomé bilayers [14], and 3D pyrochlore [15, 16] lattices, there is no consensus on the microscopic origin of the observed spin excitation continuum. In the 2D $S = 1/2$ Kagomé lattice $\text{ZnCu}_3(\text{OD})_6\text{Cl}_2$ [11] and an effective $S = 1/2$ triangular lattice magnet YbMgGaO_4 [12, 13], different interpretation of the observed spin excitation continuum includes a spin glass state of magnetic [17] and nonmagnetic Mg-Ga site disorder due to intrinsic sample issues [18, 19], respectively, rather than the fractionalized quasiparticles of a QSL [5]. To conclusively identify the presence of deconfined spinon excitations in a QSL, one needs to search for the expected spin excitation continuum among candidate QSL materials with high quality single crystals and establish their physical properties with clear experimental signatures and structures.

Recently, geometrically frustrated 2D triangular-lattice rare-earth-based materials with effective $S = 1/2$ local moments have attracted considerable attentions [20, 21]. Compared with the previous example YbMgGaO_4 [22], the family of Yb dichalcogenide delafossites NaYbCh_2 (Ch=O, S, Se) does not have the issue of Mg-Ga charge disorders in the non-magnetic layers and thus provide a genuine example for an interacting spin-1/2 triangular lattice antiferromagnet [23–25]. The combination of the strong spin-orbit coupling (SOC) and the crystal electric field (CEF) leads to a Kramers doublet ground state for the Yb^{3+} ion in NaYbCh_2 that gives rise to the effective spin-1/2 local moment at each ion site. Since the energy gaps between the ground and first excited Kramers doublets CEF levels for NaYbSe_2 [Fig. 1(b)] [26], NaYbS_2 [24], and NaYbO_2 [25] are well above ~ 12 meV, the magnetic properties below 100 K can be safely interpreted from the interaction between the effective $S = 1/2$ local moments. Although previous experiments on powder samples of NaYbO_2 provided some positive evidence for QSL ground states [24, 27, 28], there are no detailed neutron scattering experiments on single crystalline samples to establish the presence of the magnetic excitation continuum and further reveal its wave vector, energy, temperature dependence. Our result in this paper is to fulfill this goal. Here we report magnetic, heat capacity, and neutron scattering

results on single crystals of NaYbSe₂. In addition to confirming the absence of long-range magnetic order down to 40 mK, we show the presence of a spin excitation continuum extending from 0.1 to 2.5 meV. Since our careful X-ray diffraction experiments reveal only $\sim 4.8\% \pm 1\%$ of Yb on Na site and no evidence for a spin glass state at 40 mK, we conclude that the ground state of NaYbSe₂ has signatures of a QSL, consistent with the expectation of a spinon Fermi surface quantum spin liquid state [29, 30].

Results. High quality single crystals of NaYbSe₂ were grown by using flux method with Te as the flux (see Methods for further synthesis and experimental details). Figure 1(a) displays schematics of crystal structure and reciprocal space of NaYbSe₂, where Yb ions form a perfect triangular lattice layer. Inelastic neutron scattering spectra of CEF excitations obtained by subtracting the scattering of NaYbSe₂ from a non-magnetic reference NaYSe₂ is shown in Fig. 1(b) [29]. Consistent with previous work [26], the CEF levels of Yb³⁺ have a Kramers doublet ground state and three excited Kramers doublets at $E = 15.7, 24.5,$ and 30.2 meV at $T = 13$ K, thus ensuring that all measurements below about 100 K can be safely considered as an effective $S = 1/2$ ground state [26]. To characterize the behavior of the local moments of Yb and their exchange interactions, we measured the magnetic susceptibility of single-crystalline NaYbSe₂. The temperature dependence of magnetization and the in-plane magnetic susceptibility $\chi_{\perp}(T)$ is depicted in Fig. 1(c), and a simple fit to the Curie-Weiss law yields $\Theta_{CW,\perp} \simeq -13$ K in the low-temperature region (< 20 K), whose absolute value is larger than $|\Theta_{CW,\perp}| \simeq 3.5$ K when the Van Vleck contribution is subtracted [31], indicating the predominantly antiferromagnetic spin interactions in NaYbSe₂. Heat capacity measurements were also performed to characterize the thermodynamics of NaYbSe₂, and the pure magnetic contribution $C_{\text{mag}}(T)$ to the specific heat of NaYbSe₂ and its dependence on applied magnetic fields from 0 T to 8 T are presented in Fig. 1(d). The data shows a broad peak that shifts upward in temperature as a function of increasing magnetic field for $H \parallel c$, no sharp anomaly indicative of the onset of long-range order, consistent with the susceptibility result and earlier work [31]. Figure 1(e) also shows the estimated temperature dependence of $C_{\text{mag}}(T)/T$ (left axis) and the corresponding magnetic entropy S_{mag} (right axis). It is noted that $C_{\text{mag}}(T)/T$ in the low-temperature regime (< 0.5 K) is almost a constant, well compatible with the fact that the spinon Fermi surface alone has a constant density of states and would give a heat capacity depending linearly on temperature. Moreover, the temperature dependence of the magnetic entropy saturates to a value close to $S_{\text{mag}} \approx R \ln 2$ (where R is the ideal gas constant) around 15 K, consistent with an effective spin-1/2 description of the Yb³⁺ local moment [31].

Although stoichiometric NaYbSe₂ has no intrinsic structural disorder in the Na⁺ intercalating layer [23–25], real crystal could still have structural defects in Na⁺ and Se²⁻ sites, and these vacant sites could be replaced by Yb³⁺ and Te²⁻, respectively (see Methods). To accurately determine the stoichiometry of our NaYbSe₂, we carried out single crystal X-ray structural refinement by recording 1334 Bragg reflections,

corresponding to 238 non-equivalent reflections. The Rietveld refinement results of the single-crystal X-ray diffraction data collected at $T = 250$ K are shown in Fig. 1(f) and the fitting outcome reveals full occupancy of the Yb^{3+} ($3a$) and Se^{2-} ($6c$) sites in the YbSe_2 layers and $\sim 4.8\% \pm 1\%$ of the Na ($3b$) sites occupied by the Yb ions. These results are consistent with inductively-coupled plasma measurements of chemical composition of the sample (see method for details).

In the previous inelastic neutron scattering measurements on single crystals of CsYbSe_2 ($\Theta_{\text{CW}} \simeq -13$ K), spin excitations were found to be centered around the K point in reciprocal space [Fig. 1(a)], with no intensity modulation along the c -axis, and extending up to 1 meV [32]. To determine what happens in NaYbSe_2 , we must first determine if the system has long/short-range magnetic order. For this purpose, we align the crystals in the $[H, H, 0] \times [0, 0, L]$ and $[H, 0, 0] \times [0, K, 0]$ zones [Fig. 1(a)]. Figures 2(a) and 2(b) display maps of elastic scattering in the $[H, H, L]$ and $[H, K, 0]$ planes, respectively, at $T = 40$ mK (top panels) and 40 mK–10 K (bottom panels). In both cases, no evidence of long/short magnetic order was observed at 40 mK, consistent with previous magnetic, heat capacity, and nuclear magnetic resonance measurements [31]. The wave vector dependence of the spin excitations of $E = 0.3 \pm 0.1$ meV in the $[H, H, L]$ zone at 40 mK (left panel) and 10 K (right panel) is presented in Fig. 2(c). At 40 mK, one can see a featureless rod of scattering along the $[1/3, 1/3, L]$ direction, indicating that spin excitations in NaYbSe_2 are 2D in nature and have no c -axis modulations. The scattering essentially disappears at 10 K, thus confirming the magnetic nature of the scattering at 40 mK. Moreover, Fig. 2(d) shows the temperature dependence of the $E = 0.3 \pm 0.1$ meV spin excitations in the $[H, K, 0]$ zone. The magnetic scattering is centered around the K point, consistent with the previous work [32], and decreases significantly with increasing temperature.

To further reveal the intrinsic quantum dynamics of the local moments of the Yb ions, we perform the inelastic neutron scattering measurements to study the spin excitations in single crystals of NaYbSe_2 at both 40 mK and 10 K. Constant-energy images of spin excitations with a variety of energies in the in-plane 2D Brillouin zones at 40 mK and 10 K are summarized in Figs. 3(a-d) and 3(e-h), respectively. At $E = 0.15 \pm 0.05$ meV and 40 mK, the magnetic scattering spectral weights spread broadly in the Brillouin zone but with higher intensity at the K point and no scattering near the zone center (the Γ point) [Fig. 3(a)]. This is clearly different from the wave vector dependence of the low-energy magnetic scattering for YbMgGaO_4 , in which the spectral weight is enhanced around the M point [12]. The high intensity at the K point in NaYbSe_2 might arise from the strong XY -type exchange interaction, since the strong SOC in this material indeed brings certain anisotropic interactions. With increasing energies to $E = 0.6 \pm 0.1$ [Fig. 3(b)], 1.1 ± 1 [Fig. 3(c)], and $E = 2.1 \pm 0.1$ meV [Fig. 3(d)], the magnetic scattering spectral weights become more evenly distributed in the Brillouin zone and gradually decrease with increasing energy. While

the spin excitation continuum at $E = 0.15 \pm 0.05$ meV nearly vanishes on warming from 40 mK to 10 K [Fig. 1(e)], the spectral weights at other energies become weaker but are still located around the Brillouin zone boundaries, especially the scattering at the K points [Figs. 3(f-g)].

Figures 4(c) and 4(d) display the wave vector-energy dependence of the spin excitation spectral intensity (in log scale) along the magenta color arrow direction in Fig. 4(a) at 40 mK and 10 K, respectively. In both cases, the spectral intensity is broadly distributed in the energy-momentum plane, and the excitation intensity gradually decreases with increasing energy and finally vanishes above ~ 2.2 meV. The broad neutron-scattering spectral intensity at 40 mK persists to the lowest energy that we measured implying a high density of spinon scattering states at low energies. Moreover, the spectral weight around Γ point is suppressed to form a V-shaped upper bound. Combining these two facts, it strongly suggests a spinon Fermi surface QSL since this scenario not only provides a high density of spinon states near the Fermi surface, but also well explains the V-shaped upper bound on the excitation energy near the Γ point [30]. It is also noted that the low-energy spin excitations clearly peak around the K point at 40 mK [Fig. 4(c)], and they decrease dramatically on warming but still keep the V-shaped upper bound around Γ point at 10 K [Fig. 4(d)]. In addition, Figs. 4(e) and 4(f) present the wave vector-energy dependence of the spin excitation spectral intensity along the magenta color arrow directions in Fig. 4(b) at 40 mK and 10 K, respectively. The main results are similar to that in Figs. 4(c) and 4(d), and also support a spinon Fermi surface QSL.

The data points in Figs. 5(a) and 5(b) show energy dependence of spin excitations at the K_1 and M_2 points, respectively, under a variety of temperatures $T = 40$ mK, 2 K, and 10 K. The solid lines in the figures display similar data at the Γ_1 point. Consistent with Fig. 4, magnetic scattering clearly decreases with increasing temperature at the K_1 and M_2 points, and essentially vanishes at the Γ_1 point. The temperature differences (40 mK–10 K) of the imaginary part of the dynamic susceptibility, $\chi''(E)$, at the K_1 and M_2 points peak around 0.15 and 0.3 meV, respectively, as shown in the inset in Fig. 5(b). Besides, Fig. 5(c) compares energy dependence of the magnetic scattering at the M_1 , M_2 , and K_1 with the background at the Γ_2 point. To show the wave vector dependence of spin excitations, Figs. 5(d-g) plot the spectral intensity along the $[H, H, 0]$ direction for various energies of $E = 0.25 \pm 0.1$, 0.5 ± 0.1 , 1.3 ± 0.1 , and 2.3 ± 0.1 meV, respectively, at $T = 40$ mK, 2 K, and 10 K. Similarly, Figs. 5(h) and 5(i) also plot constant-energy cuts along the $[0.5 - K, 0.5 + K, 0]$ direction for energies of $E = 0.3 \pm 0.1$, 0.9 ± 0.1 , 1.5 ± 0.1 , 2.3 ± 0.1 meV at 40 mK and 10 K, respectively. All the results are compatible with Figs. 4(c-f).

Discussion and Conclusion. Overall, the magnetic and heat capacity measurements, combined with the neutron scattering results on single crystals of NaYbSe₂ demonstrate the absence of long-range magnetic order even down to 40 mK, implying a quantum disordered QSL state. In particular, besides the naive disorder and the simple spectral continuum of spin excitation, the almost linear temperature dependence of

magnetic heat capacity $C_{\text{mag}}(T)$ at the low temperature regime, the enormous low energy gapless excitations and the V-shaped upper bound around the Γ point in inelastic neutron scattering spectrum all strongly indicate the existence of a spinon Fermi surface. Theoretically, although the pure compact $U(1)$ gauge theory in two spatial dimensions is always confined due to the non-perturbative instanton events [33], it has been shown and understood that in the presence of spinon Fermi surface and gapless excitations, the QSL phase could be stable against gauge fluctuations, and a noncompact $U(1)$ gauge theory remains to be a good low energy description [8, 34]. Therefore, our experimental results and conclusion about spinon Fermi surface QSL can be compatible with theory. The scenario of spinon Fermi surface QSL could further be verified by low temperature thermal transport measurement, which has an advantage to unveil the nature of low-energy itinerant excitations.

Very recently, the pressure-induced insulator to metal transition followed by an emergence of superconductivity in NaYbSe_2 was observed in experiments [35]. This is quite remarkable since the QSL has long been thought to be a parent state of the high temperature superconductors [6–8]. It was suggested that doping a QSL could naturally result in superconductivity [6–8] due to the intimate relationship between high temperature superconductor and QSL, but the definitive experimental evidence showing that doping QSLs give rise to superconductivity is still lacking. Instead of doping, Ref. [35] obtained the superconductivity by pressure, which opens up a promising way to study the superconductivity in QSL candidates and sheds light on the mechanism of high temperature superconductivity.

* Electronic address: gangchen.physics@gmail.com

† Electronic address: guoyf@shanghaitech.edu.cn

‡ Electronic address: luxy@bnu.edu.cn

§ Electronic address: pdai@rice.edu

- [1] Anderson, P. W. Resonating valence bonds: A new kind of insulator? *Mater. Res. Bull.* **8**, 153 (1973).
- [2] Balents, L. Spin liquids in frustrated magnets. *Nature* **464**, 199-208 (2010).
- [3] Zhou, Y., Kanoda, K. and Ng, T.-K. Quantum spin liquid states. *Rev. Mod. Phys.* **89**, 025003 (2017).
- [4] Savary, L. and Balents, L. Quantum spin liquids: a review. *Rep. Prog. Phys.* **80**, 016502 (2017).
- [5] Broholm, C. *et al.* Quantum spin liquids. *Science* **367**, eaay0668 (2020).
- [6] Anderson, P. W. The resonating valence bond state in La_2CuO_4 and superconductivity. *Science* **235**, 1196-1198 (1987).
- [7] Lee, P. A., Nagaosa, N. and Wen, X. G. Doping a Mott insulator: physics of high-temperature superconductivity. *Rev. Mod. Phys.* **78**, 17-85 (2006).
- [8] P. A. Lee, From high temperature superconductivity to quantum spin liquid: progress in strong correlation

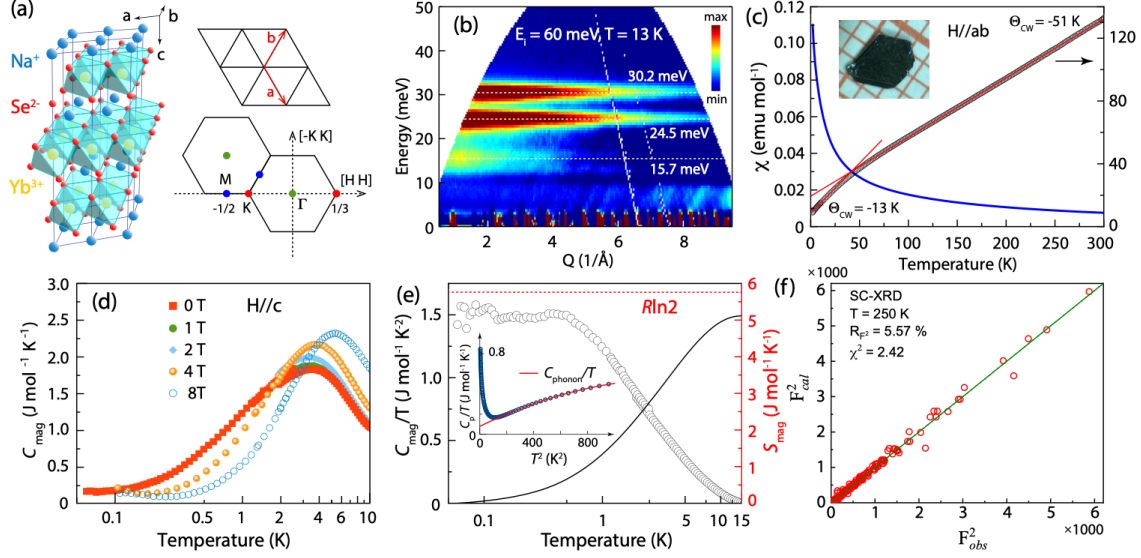


FIG. 1: Crystal structure and reciprocal space, CEF levels and heat capacity of NaYbSe₂. (a) The structure of NaYbSe₂ and corresponding reciprocal space. The lattice parameters are $a = b \approx 4.07 \text{ \AA}$, $c \approx 20.77 \text{ \AA}$. (b) Inelastic neutron scattering spectra of CEF excitations obtained by subtracting the scattering of NaYbSe₂ from a non-magnetic reference NaYSe₂. Three CEF energy levels are marked by white dashed lines. (c) Temperature-dependent magnetization along $H \perp c$ direction. The fitting for high-temperature range ($\sim 160 - 300\text{K}$) results in a Curie-Weiss temperature $\Theta_{\text{CW},\perp} \approx -51\text{K}$, and the low temperature range ($< 20\text{K}$) generates a $\Theta_{\text{CW},\perp} \approx -13\text{K}$. The inset shows the crystal for the magnetization measurements. (d) Contribution of magnetic component (C_{mag}) to the specific heat of NaYbSe₂ and its dependence on applied magnetic field $H \parallel c$. Phonon contribution has been subtracted. (e) Temperature dependent C_{mag}/T (black circle) and the magnetic entropy (black curve). The red dashed line marks the value of $R \ln 2$. The inset shows C_p/T as a function of T^2 . The red solid curve is a fitting of the phonon contribution C_{phonon} . (f) The Rietveld refinement results of the single-crystal X-ray diffraction data at 250 K yield Na_{0.952(10)}Yb_{0.048(10)}YbSe₂. F_{cal}^2 and F_{obs}^2 are the calculated and observed structure factors, respectively.

physics, Reports on Progress in Physics. **71**, 012501 (2007).

- [9] Kitaev, A. Y. Fault-tolerant quantum computation by anyons. Ann. Phys. **303**, 2-30 (2003).
- [10] Kitaev, A. Anyons in an exactly solved model and beyond. Ann. Phys. **321**, 2-111 (2006).
- [11] Han, T. H. *et al.* Fractionalized excitations in the spin-liquid state of a kagome-lattice antiferromagnet. Nature **492**, 406-410 (2012).
- [12] Shen, Y. *et al.* Evidence for a spinon Fermi surface in a triangular-lattice quantum-spin-liquid candidate, Nature (London) **540**, 559 (2016).
- [13] Paddison, J. A. M. *et al.* Continuous excitations of the triangular-lattice quantum spin liquid YbMgGaO₄, Nat. Phys. **13**, 117 (2017).
- [14] Balz, C. *et al.* Physical realization of a quantum spin liquid based on a complex frustration mechanism. Nat. Phys. **12**, 9421 7949 (2016).

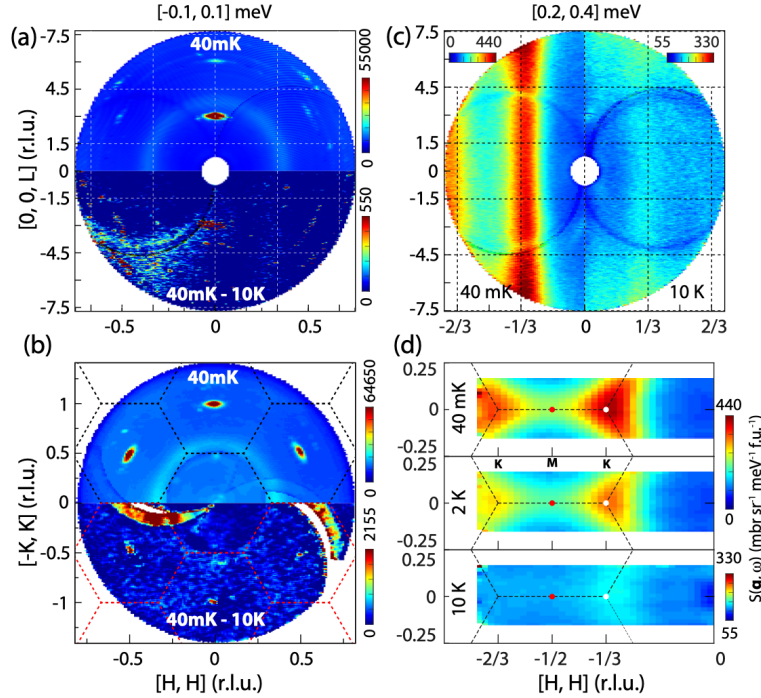


FIG. 2: **Neutron scattering results in $[H, H, L]$ and $[H, K, 0]$ zones.** Elastic neutron scattering results ($E = 0 \pm 0.1$ meV) in (a) the $[H, H, L]$ plane and (b) $[H, K, 0]$ plane measured with $E_i = 3.32$ meV and 3.70 meV, respectively. Scattering along the vertical direction ($[-K, K, 0]$ for (a) and $[0, 0, L]$ for (b)) is integrated. The upper half panels of (a) and (b) are data at $T = 40$ mK, and the lower are the differences between $T = 40$ mK and 10 K. (c) L -dependence of the spin excitations along the $[H, H]$ direction at $T = 40$ mK (left half panel) and $T = 10$ K (right half panel), with $K = [-0.05, 0.05]$ and $E = 0.3 \pm 0.1$ meV. (d) Spin excitations with $E = 0.3 \pm 0.1$ in the $[H, K]$ plane measured at $T = 40$ mK, 2, and 10 K. Scattering along the $[0, 0, L]$ direction is integrated. The black dashed lines mark the Brillouin zones of NaYbSe_2 .

- [15] Gao, B. *et al.* Experimental signatures of a three-dimensional quantum spin liquid in effective spin-1/2 $\text{Ce}_2\text{Zr}_2\text{O}_7$ pyrochlore. *Nat. Phys.* **15**, 1052-1057 (2019).
- [16] Gaudet, J. *et al.* Quantum spin ice dynamics in the dipole-octupole pyrochlore magnet $\text{Ce}_2\text{Zr}_2\text{O}_7$. *Phys. Rev. Lett.* **122**, 187201 (2019).
- [17] Freedman, D. E. *et al.* Site specific X-ray anomalous dispersion of the geometrically frustrated kagomé magnet, herbertsmithite, $\text{ZnCu}_3(\text{OH})_6\text{Cl}_2$. *J. Am. Chem. Soc.* **132**, 161851-16190 (2010).
- [18] Ma, Z. *et al.* Spin-glass ground state in a triangular-lattice compound YbZnGaO_4 , *Phys. Rev. Lett.* **120**, 087201 (2018).
- [19] Zhu, Z., Maksimov, P. A., White, S. R., and Chernyshev, A. L. Disorder-induced mimicry of a spin liquid in YbMgGaO_4 , *Phys. Rev. Lett.* **119**, 157201 (2017).
- [20] Rau, J. G. and Gingras, M. J. P. Frustration and anisotropic exchange in ytterbium magnets with edge-shared octahedra, *Phys. Rev. B* **98**, 054408 (2018).
- [21] Maksimov, P. A., Zhu, Z., White, S. R., and Chernyshev, A. L., Anisotropic-exchange magnets on a triangular

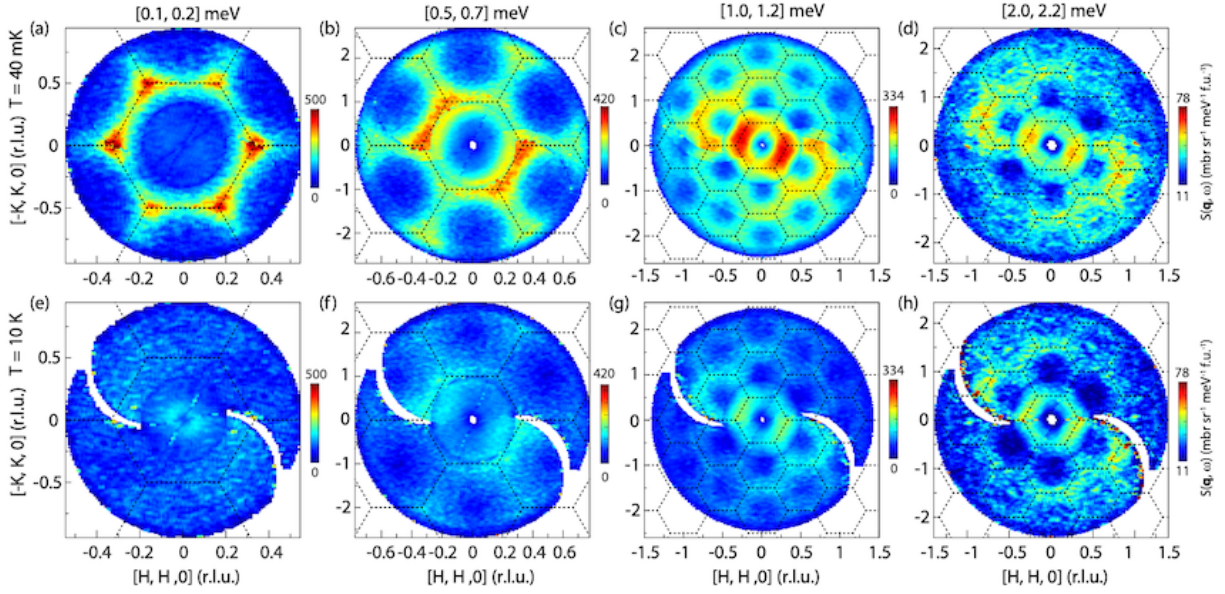


FIG. 3: **Constant-energy images of spin excitations in the $[H, K, 0]$ plane.** (a-d) Images at $T = 40$ mK and (e-h) 10 K. The intensity along the vertical $[0, 0, L]$ direction is integrated. Spin excitations for (a,e) $E = 0.15 \pm 0.05$, (b,f) 0.5 ± 0.1 , (c,g) 1.1 ± 0.1 , and (d,h) 2.1 ± 0.1 meV are measured with $E_i = 1.77, 3.70, 12.14$ and 12.14 meV, respectively. The black dashed lines mark the Brillouin zones in the reciprocal space. The data are collected in 180° range of sample rotation around the $c - axis$. The 360° circular coverage are generated by averaging the raw data and its mirror in the $[H, K, 0]$ plane.

lattice: spin waves, accidental degeneracies, and dual Spin Liquids, Phys. Rev. X **9**, 021017 (2019).

- [22] Li, Y. *et al.* Gapless quantum spin liquid ground state in the two-dimensional spin-1/2 triangular antiferromagnet YbMgGaO_4 , Sci. Rep. **5**, 16419 (2015).
- [23] Liu, W. *et al.* Rare-earth chalcogenides: A large family of triangular lattice spin liquid candidates, Chin. Phys. Lett. **35**, 117501 (2018).
- [24] Baenitz, M. *et al.* NaYbS_2 : A planar spin-1/2 triangular-lattice magnet and putative spin liquid, Phys. Rev. B **98**, 220409(R) (2018).
- [25] Ranjith, K. M. *et al.* Field-induced instability of the quantum spin liquid ground state in the $J_{eff} = 1/2$ triangular-lattice compound NaYbO_2 , Phys. Rev. B **99**, 180401(R) (2019).
- [26] Zhang, Z. *et al.* Crystalline Electric-Field Excitations in Quantum Spin Liquids Candidate NaYbSe_2 , arXiv:2002.04772.
- [27] Bordelon, M. M. *et al.* Field-tunable quantum disordered ground state in the triangular-lattice antiferromagnet NaYbO_2 , Nat. Phys. **15**, 1058 (2019).
- [28] Ding, L. *et al.* Gapless spin-liquid state in the structurally disorder-free triangular antiferromagnet NaYbO_2 , Phys. Rev. B **100**, 144432 (2019).
- [29] See supplementary information for details.
- [30] Li, Y. D., Lu, Y. M., and Chen, G., Spinon Fermi surface $U(1)$ spin liquid in the spin-orbit-coupled triangular-

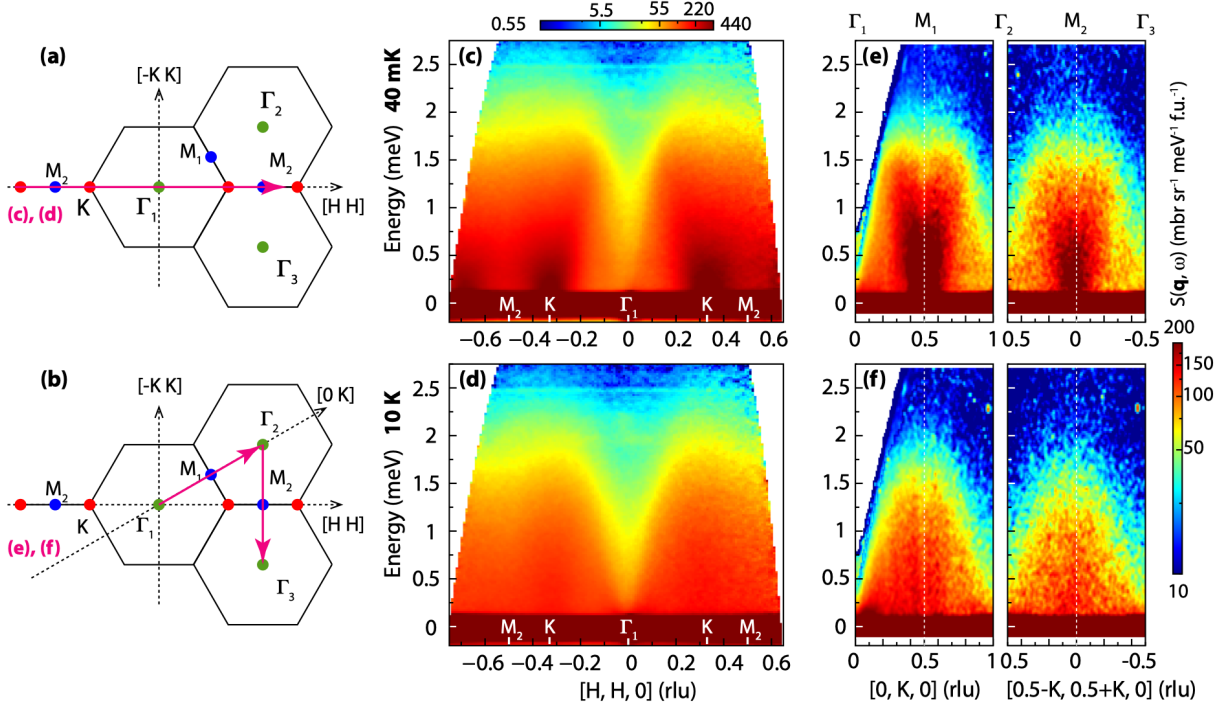


FIG. 4: **Spin excitation spectra along high symmetry momentum directions.** (a,b) Schematics of the Brillouin zones with high symmetry points Γ , K , and M denoted by green, red, and blue dots, and the high symmetry directions for the images in (c-f) marked by pink lines with arrow heads. Spin excitation spectra collected at (c) $T = 40$ mK and (d) 10 K along the $M_2-K-\Gamma-K-M_2$ with $E_i = 3.32$ meV. (e,f) Intensity color maps along the $\Gamma_1-M_1-\Gamma_2$ and $\Gamma_2-M_2-\Gamma_3$ directions measured with $E_i = 3.7$ meV.

lattice Mott insulator YbMgGaO_4 , Phys. Rev. B **96**, 054445 (2017).

- [31] Ranjith, K. M. *et al.* Anisotropic field-induced ordering in the triangular-lattice quantum spin liquid NaYbSe_2 , Phys. Rev. B **100**, 224417(R) (2019).
- [32] Xing, J. *et al.* Field-induced magnetic transition and spin fluctuations in the quantum spin-liquid candidate CsYbSe_2 , Phys. Rev. B **100**, 220407(R) (2019).
- [33] Polyakov, A. M., Quark confinement and topology of gauge theories, Nucl. Phys. B **120**, 429 (1977).
- [34] Lee, S. S., Stability of the $U(1)$ spin liquid with a spinon Fermi surface in $2 + 1$ dimensions, Phys. Rev. B **78**, 085129 (2008).
- [35] Jia, Y. *et al.* Mott Transition and Superconductivity in Quantum Spin Liquid Candidate NaYbSe_2 , arXiv:2003.09859, (2020).
- [36] Rodríguez-Carvajal, J. Recent advances in magnetic structure determination by neutron powder diffraction. Phys. B **192**, 55-69 (1993).
- [37] Ehlers, G. *et al.* The new cold neutron chopper spectrometer at the Spallation Neutron Source: Design and performance, Rev. Sci. Instrum. **82**, 085108 (2011).
- [38] Abernathy, D. L. *et al.*, Design and operation of the wide angular-range chopper spectrometer ARCS at the

- Spallation Neutron Source, *Rev. Sci. Instrum.* **83**, 015114 (2012);
- [39] Bewley, R. I. *et al.* LET, a cold neutron multi-disk chopper spectrometer at ISIS, *Nuclear Instruments and Methods in Physics Research A* **637**, 128 (2011).
- [40] Lu, X. *et al.*; (2020): Fractionalized magnetic excitations in a quantum spin liquid candidate NaYbSe₂, STFC ISIS Neutron and Muon Source, <https://doi.org/10.5286/ISIS.E.RB1920512>.
- [41] Arnold, O. *et al.* Mantid—Data analysis and visualization package for neutron scattering and μ SR experiments, *Nuclear Instruments and Methods in Physics Research A* 764, 156 (2014).
- [42] Ewings, R. A. *et al.* HORACE: Software for the analysis of data from single crystal spectroscopy experiments at time-of-flight neutron instruments, *Nuclear Instruments and Methods in Physics Research A* **834**, 132 (2016).

Acknowledgments We thank M. Stone for suggestions of appropriate neutron scattering instrumentation, and Feng Ye (ORNL) for the assistance with the single-crystal x-ray diffraction measurements. The research at Beijing Normal University is supported by the National Natural Science Foundation of China (Grant No. 11734002 and 11922402, X.L.). The work at ShanghaiTech university is supported by the National Natural Science Foundation of China (No. 11874264, Y.G.). Y.G. and X.W. thank the support from Analytical Instrumentation Center (# SPST-AIC10112914), SPST, ShanghaiTech University. The neutron scattering work at Rice is supported by US DOE BES DE-SC0012311 (P.D.). This work is further supported by funds from the Ministry of Science and Technology of China (grant No.2016YFA0301001, No.2018YFGH000095, No.2016YFA0300500 for G.C., and No.2016YFA0300501, No.2016YFA0300503 for L.S. and G.C.) and from the Research Grants Council of Hong Kong with General Research Fund Grant No.17303819 (G.C.). E.F. and H.C. acknowledges support of US DOE BES Early Career Award KC0402010 under Contract DE-AC05-00OR22725. E.M. and C.-L.H. acknowledge support from US DOE BES DE-SC0019503. This research used resources at Spallation Neutron Source, a DOE Office of Science User Facility operated by ORNL. We gratefully acknowledge the Science and Technology Facilities Council (STFC) for access to neutron beamtime at ISIS.

Methods

Crystal Growth NaYbSe₂ single crystals were grown by using Te as the flux. The starting materials are in a molar ration of Na : Yb : Se : Te = 1 : 1 : 2 : 20. To avoid the violent reaction between Na and Se, the Na (99.7%) blocks and Te (99.999%) granules were mixed and slowly heated up to 200°C within 20 hours and pre-reacted at the temperature for 10 hours. The precursor was then thoroughly mixed with Yb (99.9%) blocks and Se (99.999%) granules in the molar ratio and placed into an alumina crucible. The crucible was sealed into a quartz tube under the vacuum of 10⁻⁴ Pa and then slowly heated up to 950°C within 15 hours. After the reaction at this temperature for 20 hours, the assembly was slowly cooled down to 800°C at a temperature decreasing rate of 1°C/h. At 800°C, the quartz tube was immediately taken out of the furnace and placed into a high-speed centrifuge to separate the excess Te flux. To show a comparison,

NaYbSe₂ crystals were also grown by using NaCl as the flux in the similar procedure as mentioned above. The crystallographic phase and quality of the grown crystals were examined on a Bruker D8 VENTURE single crystal X-ray diffractometer using Mo K_{α1} radiation ($\lambda = 0.71073\text{\AA}$) at room temperature. The crystals grown by using different flux have the same high quality. Growth of the polycrystalline NaYbSe₂ and NaYSe₂ samples has been described elsewhere [31].

Stoichiometric Analysis The single crystal X-ray diffraction of NaYbSe₂ were performed at 250 K on Rigaku XtaLAB PRO diffractometer at Spallation Neutron Source, ORNL. Structure refinement based on the X-ray diffraction data were carried out with FullProf suite [36], generating (Na_{0.952(10)}Yb_{0.048(10)})YbSe₂ without Te occupying Se sites. Elemental analysis of a group of NaYbSe₂ single crystals grown with Te flux with a total mass of 35mg were performed by inductively-coupled plasma (ICP) method on Thermo Fisher ICP 7400 system. The result—Na_{0.965}Yb_{1.03}Se_{1.98}Te_{0.025}—can be interpreted as $\sim 3\%$ of Na⁺ sites being occupied by Yb ions and agrees well with the structure refinement results of single-crystal x-ray diffraction, especially considering that Te could exist as flux in the sample.

Heat Capacity The specific heat capacity of NaYbSe₂ was measured down to 50 mK using a thermal-relaxation method in DynaCool-PPMS (Physical Property Measurement System, Quantum Design) with the magnetic field applied along the *c*-axis at Fudan University and Rice University. The total specific heat is described as a sum of magnetic and lattice contributions: $C_p = C_{\text{mag}} + C_{\text{phonon}}$. We fit the phonon contribution with $C_{\text{phonon}} = \beta T^3 + \alpha T^5$.

Neutron Scattering The neutron scattering measurements of the magnetic excitations in [H, H, L] scattering plane, and the CEF excitations were performed on the Cold-Neutron-Chopper-Spectrometer (CNCS) [37] and ARCS [38] at the Spallation Neutron Source (SNS), Oak-Ridge National Laboratory (ORNL), respectively. The measurements in [H, K, 0] scattering plane were carried out on the LET cold neutron chopper spectrometer [39], ISIS spallation neutron source, Rutherford Appleton Laboratory (RAL), UK. We co-aligned ~ 3.7 grams of NaYbSe₂ single crystals for the measurements of magnetic excitations and prepared ~ 10 grams NaYbSe₂ and NaYSe₂ polycrystalline samples for the CEF excitation measurements. The neutron scattering data was reduced with Mantid [41] and analyzed with Mantidplot, Horace [42], and Mslice.

Author Contributions P.-L.D. and G.Z. contribute equally to this work. X.L., Y.G., and P.D. conceived this project. P.-L.D., G.T. and X.L. applied the beamtimes. G.Z. and Y.G. prepared the samples and did basic structure and magnetic characterizations with the help from S.W. and X.W.. E.F. and H.C. did X-ray structure refinement. Z.Z., C.-L.H., E.M. and L.S. performed the specific heat measurements. Z.Z. and L.S. analyzed the specific heat data. P.-L.D., X.L., Y.F.X. and C.D. performed neutron scattering experiments on CNCS, LET, and ARCS spectrometers with the help from A.P., G.E.G., and D.V.. P.-L.D. and X.L. analyzed

the neutron scattering data and prepared the figures. Y.H.G. and G.C. provided the physical interpretation of the results. X.L., Y.H.G., G.C. and P.D. wrote the manuscript with input from Y.G.. All authors made comments.

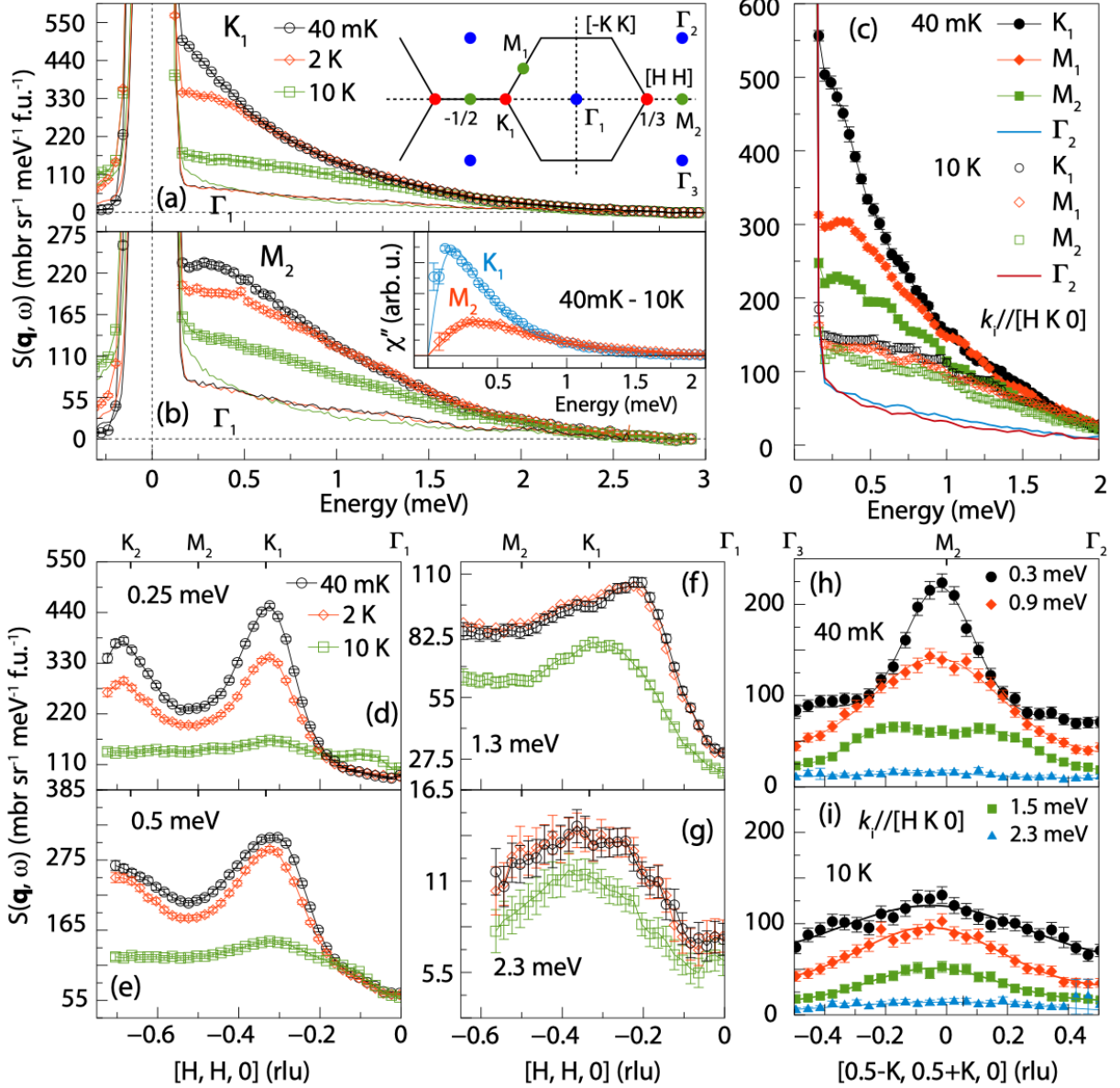


FIG. 5: **Wave vector dependence of spin excitations along high symmetry directions.** The wave vector cuts in (a,b,d-g) were measured in the $[H, H, L]$ zone, while those in (c,h,i) were measured in the $[H, K, 0]$ plane. (a) and (b) show the energy dependent scattering at K_1 and M_1 points measured at $T = 40$ mK (black circle), 2 K (red diamond) and 10 K (green square). The inset in (a) is a schematic of the reciprocal space with the Γ , K and M points denoted by green, red and blue dots. The black, red, and green curves are energy cuts at Γ_1 . The inset of (b) shows the difference of χ'' between the spectra for $T = 40$ mK and 10 K at the K and M points. The light blue and red curves are fittings of the χ'' with a damped harmonic oscillator model. (c) shows the energy cuts at the K_1 , M_1 , M_2 and Γ_2 . Solid symbols represent the data collected at $T = 40$ mK and the open symbols collected at 10 K. The black and blue curves are energy cuts at the Γ_2 point measured at $T = 40$ mK and 10 K. (d-g) Constant energy cuts along the M_2 - K_1 - Γ_1 for $T = 40$ mK, 2 K, and 10 K, with corresponding energy transfers marked in the panels. Constant energy cuts along the Γ_3 - M_2 - Γ_2 measured at (h) $T = 40$ mK and (i) 10 K. The solid curves are guides to the eyes.